Assessment of the impact of localized disturbances on SI-POF transmission using a matrix propagation model

2011 J. Opt. 13 055406

(http://iopscience.iop.org/2040-8986/13/5/055406)

IOP Publishing Journal of Optics
J. Opt. **13** (2011) 055406 (6pp) doi:10.1088/2040-8978/13/5/055406

Assessment of the impact of localized disturbances on SI-POF transmission using a matrix propagation model

M A Losada, J Mateo and J J Martínez-Muro

GTF, Aragón Institute of Engineering Research (i3A), María de Luna 1, E-50018 Zaragoza, Spain

E-mail: alosada@unizar.es

Received 22 November 2010, accepted for publication 3 March 2011
Published 31 March 2011
Online at stacks.iop.org/JOpt/13/055406

Abstract
Our aim is to extend the matrix approach of the power flow equation to study the effects of different devices over light propagation in step index plastic optical fibers (SI-POFs). Here we devise an experimental method to characterize a particular scrambler as a matrix which can be directly introduced into the model framework to predict transmission properties. Thus, fiber bandwidth versus length was simulated for different scrambler configurations and then compared with experimental data to verify the characterization method. A study of the scrambler effects for different launching conditions reveals important aspects of its impact on transmission.

Keywords: step index plastic optical fiber, propagation model, transmission properties, scrambler

(Some figures in this article are in colour only in the electronic version)

1. Introduction

Transmission properties in POFs show a complex dependence on fiber length whose origin is generally attributed to strong mode coupling and cannot be explained with simple models. Due to the high multi-modality of POFs, the propagation angle can be treated as a continuous variable and optical power propagation through the fiber can be described by a differential power flow equation as proposed by Gloge [1]. Thus, there are different approaches to POF modeling based on Gloge's equation which can be used to describe optical power propagation including modal coupling [2, 3]. In fact, our method is based on this approach, introducing diffusion and attenuation as general functions of the angle [4]. These characteristic functions, that account for the particular fiber modal behavior, were estimated from experimental far-field patterns (FFPs) [4]. However, as the temporal dependence was not explicit in our equation, the frequency response and bandwidth could not be calculated. Thus, we recently proposed a fast and robust method to solve the power flow equation generalized to incorporate the temporal dimension [5–7]. This method provides the evolution of the spacetime optical power distribution with length from which angular power distribution, attenuation, bandwidth and pulse spreading can be derived. We showed that model simulations reproduce experimental measurements, such as FFPs and frequency responses [4, 7], but can also be applied to obtain predictions of fiber properties where it is difficult or impractical to measure them. In addition, we postulated that this method offers a flexible tool to study the impact of localized disturbances over transmission properties. In fact, our aim here is to show how a device or defect, providing that it is characterized by a matrix, can be straightforwardly introduced into the model framework to obtain a description of its effects over power propagation and derive the changes imposed on spatial distribution or bandwidth.

In particular, the chosen device to test our hypothesis is a corrugated scrambler that we have used before to obtain experimental frequency responses of POFs from different manufacturers [8, 9]. These measurements will be used to test the behavior of the combined model. Thus, we first present a procedure devised to obtain the characteristic matrix for this

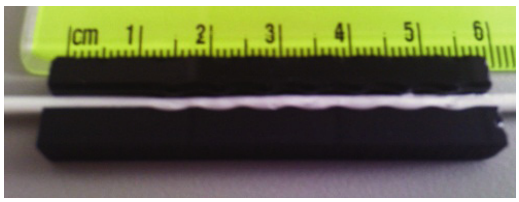

Figure 1. Corrugated scrambler designed for 1 mm POFs.

scrambler. Our method is based on comparing radial profiles extracted from output FFPs measured without the scrambler and with the scrambler near the fiber output end in order to separate its effects from those of power propagation. Then, we explain how the scrambler matrix can be easily introduced into the propagation matrix model to obtain a joint model for the scrambler–fiber system. In section 3, we evaluate the capability of this scrambler–fiber matrix model to reproduce experimental measurements of frequency bandwidth and to obtain useful predictions for practical links. In section 5, we give a summary of our conclusions that reveal the potential of the matrix approach of the power flow equation to study the effects of devices such as scramblers, tappers, etc, over light propagation in plastic optical fibers.

2. Characterization of the scrambler

In this section, we describe our method to obtain a matrix that characterizes the scrambler effects over optical power and that can be easily introduced into the propagation matrix model framework. The scrambler used in our measurements, shown in figure 1, is 5.5 cm long, has seven corrugations with a 6 mm pitch and a corrugation depth of 0.5 mm where the fiber has to be inserted [8]. To characterize the scrambler, experimental radial profiles were extracted from the FFPs for short fiber segments launching a collimated beam and scanning the input angle in the horizontal plane. The angular scan of radial profiles is obtained first without the scrambler and then with the scrambler near the fiber output end. In this way, the propagation effects are negligible and all the changes in the profiles are produced by the scrambler. The measurements with the scrambler were always taken following carefully the same procedure to insert the fiber to ensure that its behavior was reproducible. We have tested poly methyl methacrylate (PMMA) optical fibers of similar properties (1 mm diameter and high NA) from three different manufacturers: ESKA-PREMIER GH4001 (GH) from Mitsubishi, PGU-FB1000 (PGU) from Toray and HFBR-RUS100 (HFB) from Avago.

The radial profiles have been obtained from FFPs recorded for each input angle by a cooled camera following a method described in previous works [4], except for the injection module. This module consists of an He–Ne laser beam of 635 nm directly injected into the fiber input end, which is placed on the center of a motorized rotary mount in order to vary the launching angle. The FFP images, obtained for input angles varied from $-40°$ to $40°$ in $1°$ steps, were automatically registered and stored. The whole angular scan was obtained first for fiber segments of 1.25 m without the scrambler and then the same fiber segment was tested but with the scrambler inserted 10 cm from its output end. All experimental conditions (laser injection, starting angle, fiber position, etc) remained the same for both scans. Radial profile scans for the three fibers are shown in figure 2 as images.

We have used this image representation to display the profiles at all different injection angles in a single plot. In these images, each column represents the radial profile for the corresponding input angle as a function of the output angle on the vertical axis. The mirror images of the profiles, corresponding to negative output angles, are also shown for the sake of symmetry. The profiles for negative injection angles have also been measured and are not exactly the same as those obtained for the positive angles, revealing the deviations from the ideally symmetric response. The left images show radial profiles measured without a scrambler, while the middle ones show radial profiles when the scrambler was placed close to the output end. The right images show radial profiles calculated using the scrambler matrix as will be described later. To enhance the visibility of the lower power values obtained for the scrambler at high input angles, all images have been submitted to a logarithmic transform. Higher values are shown in deep red and lower values in dark blue. The scales are the same for all images, so those measurements obtained with the scrambler are dimmer, indicating power loss.

The images show how, when using the scrambler, the power is spread over a wide range of output angles and thus the narrow peaks clearly visible in the images obtained without the scrambler nearly disappear in the middle and rightmost ones. Thus, the wide power spread caused by the scrambler is equivalent to a strong mode coupling that is achieved in a very short distance. The scrambler induces power transfer not only between adjacent modes or angles, but also to others further away. We assumed the scrambler can be modeled as a linear angle-variant system, which means that the output power for a given input angle can be written as a linear combination of the power at that and other angles, variant with the input angle. Therefore, the scrambler effects can be modeled as a multiplicative matrix, $\mathbf{S}$. Thus, given the input power profile as a column vector, p_i, where each vector element is the power at a given angle, the output power vector, p_o, can be obtained by the matrix product of p_i, by the scrambler characteristic matrix, given as $p_\mathrm{o} = \mathbf{S} \cdot p_\mathrm{i}$. The images presented above can also be seen as matrices where each column is a power vector whose horizontal index represents the input angle. Thus, the effects of the scrambler over the whole dataset can be directly calculated as the matrix product:

$$\mathbf{P_o} = \mathbf{S} \cdot \mathbf{P_i}, \tag{1}$$

where $\mathbf{P_o}$ and $\mathbf{P_i}$ are matrices built as column power vector aggregates.

In the matrix $\mathbf{S}$, each column indicates the spread of the power in a given input angle due to the scrambler. Each element in the column gives the relative power transferred to the angle indicated by the row index. If power spread was independent on the input angle, the matrix product would be equivalent to a convolution of a single function by the input power vector. This, however, is not the case as the images

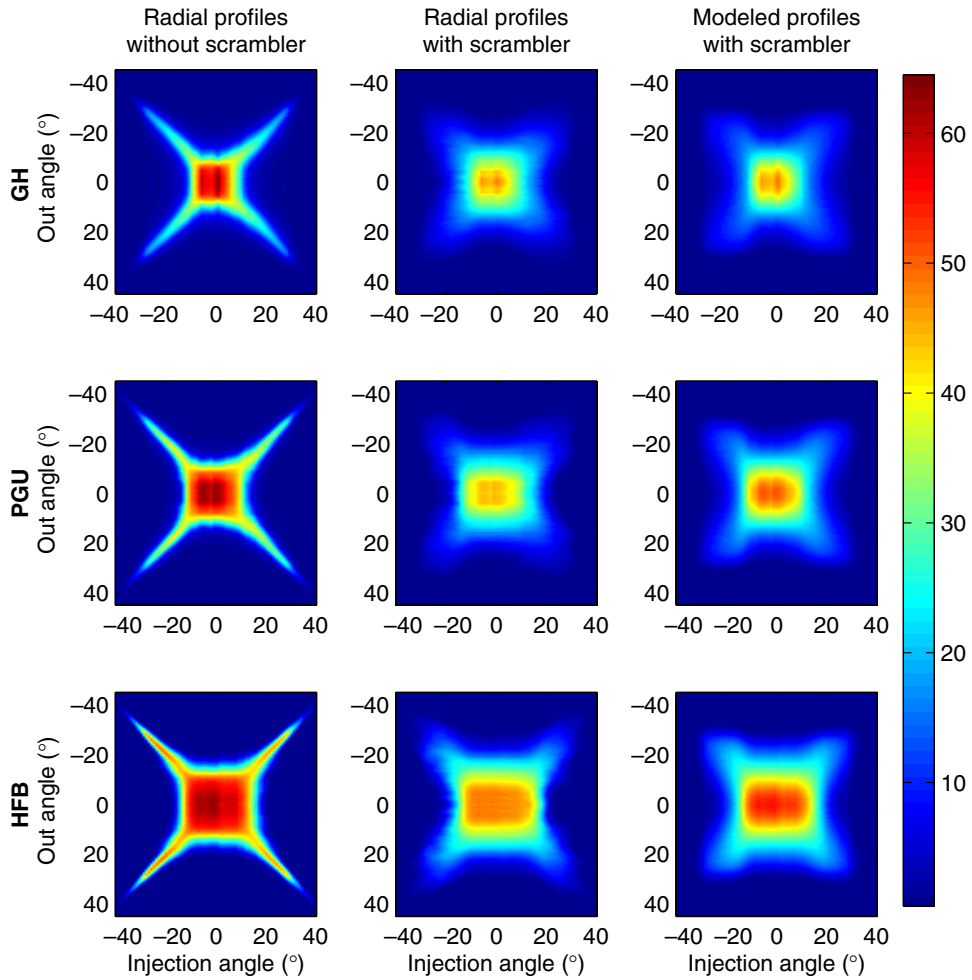

Figure 2. Radial profile images for the three tested fibers. The upper row shows data for the GH fiber, the middle row for the PGU fiber and the lower row for the HFB fiber. The leftmost images show data without the scrambler, the middle images show data with the scrambler, and the rightmost images show data predicted by the scrambler model.

show that the scrambler induces a power spread that affects a wider angular range for higher angles. Therefore, we assumed that the spread increases as a function of input angle, which is equivalent to modeling the scrambler as a linear but angle-variant system. To model this power spread we used a Gaussian whose standard deviation and center depend on the angle θ_i, as given by the following equation:

$$G(\theta_i, \theta_o) = H(\theta_i) \cdot \exp\{-((\theta_o - g \cdot \theta_i)/\sigma(\theta_i))^2\}, \qquad (2)$$

where g is a parameter to model center deviation. The function $H(\theta_i)$ accounts for the angular-dependent power loss which is modeled by a flat function of a sharp fall above 30° given by

$$H(\theta_i) = h/(1 + \exp((|\theta_i| - 28°)/2°)), \qquad (3)$$

where the parameter h represents the overall power loss. Finally, the angular-dependent width, $\sigma(\theta_i)$, is given by

$$\sigma(\theta_i) = a - b \cdot \exp(-(|\theta_i|/c)^f), \qquad (4)$$

where the parameters c and f control the rate of increase of the standard deviation with angle, while a and b determine its value at 0° and high angles, respectively. Other similar functions could be used but the Gaussian is easier to work with and gives a good agreement with the experimental behavior of the scrambler. The six free model parameters were fitted to the pooled data of the three fibers. As in the previous analysis we did not find significant differences between the sets of parameters obtained by fitting data for each fiber separately. Using equation (2) with the parameters for the best fit we obtained the matrix **S**, shown as an image in figure 3. With the matrix **S** and equation (1), we obtained the images on the right of figure 2 using the profiles shown in the left images as input $\mathbf{P_i}$. These images are quite similar to those in the middle, demonstrating that the matrix **S** gives a good account of the scrambler effects. The differences in the maximum values of the modeled and measured radial profiles are due to a difference in the overall losses for each fiber. As the scrambler parameters were obtained by fitting them to the pooled data for the three fibers, the overall attenuation obtained was a compromise for the three fibers. If the scrambler matrix is fitted to each fiber, the level can be more accurately matched but we think it more useful to have a unique scrambler model, independent of fiber type.

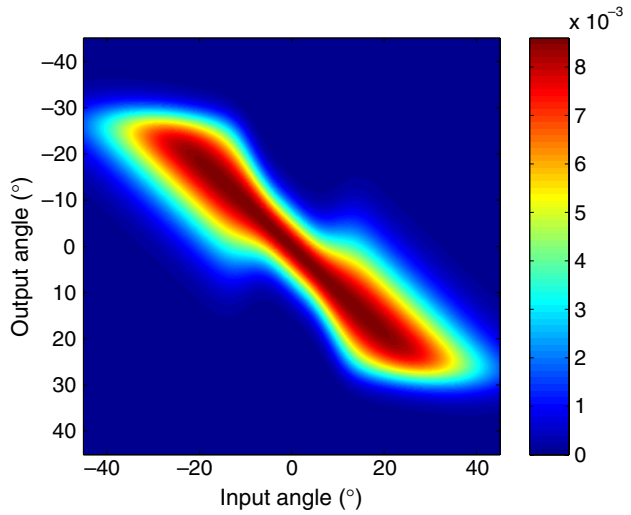

Figure 3. Image representation of the scrambler characteristic matrix, **S**, calculated using the parameters for the best fit whose values are: $a = 15°$, $b = 7.5°$, $c = 11.35°$, $g = 0.96$, $f = 3.19$ and $h = 0.0086$.

3. Joint scrambler and propagation model

Our aim here is to show the flexibility of our propagation model in matrix form to incorporate different localized effects once they have a matrix characterization such as the scrambler under study. Gloge's power flow equation describes the evolution of the modal power distribution as it is transmitted throughout a POF where different modes are characterized by their propagation angle with respect to the fiber axis (θ), considered as a continuous variable. Angular diffusion, $d(\theta)$, and attenuation, $\alpha(\theta)$, are described as functions of the propagation angle, characteristic for each fiber type, and were estimated from experimental FFPs for the three fibers used in this work [4]. To solve this differential equation we implement a finite-difference method in a matrix form where, for any pair of lengths, $z_2 > z_1$, we can put the difference equation in matrix notation as

$$\mathbf{p}(z_2, \omega) = (\mathbf{A}(\omega) + \mathbf{D})^m \cdot \mathbf{p}(z_1, \omega), \tag{5}$$

where $\mathbf{p}(z_1, \omega)$ and $\mathbf{p}(z_2, \omega)$ are column vectors giving the angular power distribution in the frequency domain at two fiber lengths, whose difference is m times the elementary length [7]. **A** is a diagonal matrix that describes power propagation without diffusion, while the tri-diagonal matrix **D**, which does not depend on frequency, accounts for fiber diffusion. These matrices are calculated from $\alpha(\theta)$ and $d(\theta)$, respectively, and thus are different for each fiber type.

This model, along with the characteristic matrix of the scrambler, **S**, is used to predict its effects on different transmission properties. The effect of the scrambler has been analyzed for two different scrambler positions: near the input end of the fiber and near its output end. Thus, the scrambler matrix has to be introduced as the right or left matrix product of **S** by the fiber propagation matrix, $(\mathbf{A}(\omega) + \mathbf{D})$, depending on whether the scrambler is at the input or at the output end, respectively, such as the following equations show:

$$\mathbf{p}(z_2, \omega) = (\mathbf{A}(\omega) + \mathbf{D})^m \cdot \mathbf{S} \cdot \mathbf{p}(z_1, \omega), \tag{6}$$

$$\mathbf{p}(z_2, \omega) = \mathbf{S} \cdot (\mathbf{A}(\omega) + \mathbf{D})^m \cdot \mathbf{p}(z_1, \omega). \tag{7}$$

From $\mathbf{p}(z, \omega)$, different transmission parameters can be obtained such as the frequency response or the output angular distribution as a function of fiber length [7]. These equations, which account for the combined effects of scrambler and fiber propagation, will be used next to test the model performance.

4. Model validation and predictions

Once we have a joint model for the device and the effects of fiber propagation, we first validate our method by comparing model predictions to our previous experimental estimates of bandwidths versus fiber length measured in [9] with the same scrambler in section 4.1. Moreover, as predictions of different parameters can be directly obtained with the model where it is not practical or easy to measure them, we present in section 4.2 an analysis of the global scrambler–fiber system behavior for different launching conditions. It is well known how, due to their large aperture, most POF properties are strongly dependent on the input source aperture and therefore different scramblers have been designed to obtain a uniform overfilled launch [8, 10–12]. Thus, we assess if the presence of a scrambler near the transmitter guarantees a similar output pattern independently from the source aperture and fiber length. In addition, it has been found experimentally that spatial filtering close to the receptor, such as that produced by a small-area detector [13] or by a small displacement of the fiber from the detector [14, 15], can improve the system behavior in general. In particular, a bandwidth increase has been reported [9, 16, 17] when placing this particular scrambler near the detector. Here, we evaluate the extent of this improvement to determine the usefulness of this or a similar scrambler in practical POF links.

4.1. Comparison to experimental bandwidth versus length data

First, we have tested the capability of our propagation model in matrix form to reproduce experimental measurements of bandwidth versus length obtained using this same scrambler. These bandwidths were extracted from experimental frequency responses measured for the same fiber types and placing the scrambler in two different positions: near the input and output end of the fiber. The experimental procedure was based on the cut-back method, starting from long fiber samples down to 10 m and was described in detail elsewhere [9]. Frequency responses were also measured without the scrambler and were correctly reproduced by the propagation model as was previously published [7]. Figure 4 shows these experimental results for the three fibers tested, red circles for the scrambler near the input end and blue squares for the scrambler near the output end. The left plot shows the bandwidth versus length for the GH, the middle for the HFB and the right plot for the PGU.

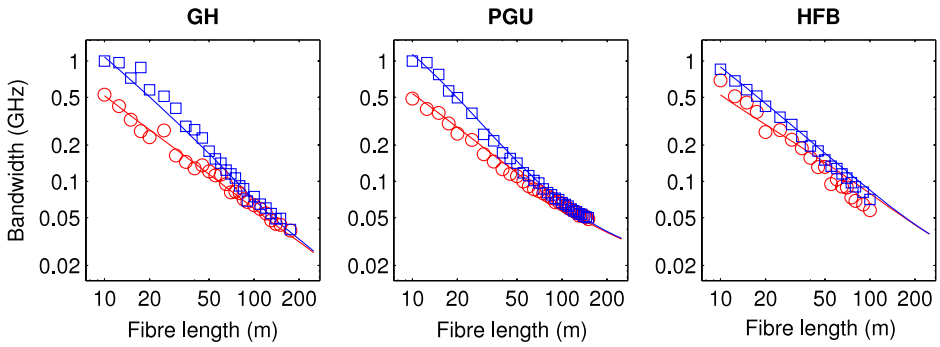

Figure 4. Comparison of experimental and model predicted bandwidth versus length with the scrambler at the transmitter (circles and red lines) and with the scrambler near the detector (squares and blue lines).

From equations (6) and (7), we calculated $\mathbf{p}(z, \omega)$ at the measured fiber lengths using the same scrambler characteristic matrix **S** for all tested fibers. However, the propagation matrix is different for each fiber as it was obtained using their characteristic angular diffusion and attenuation previously estimated from experimental radial profiles in [4]. Thus, model predictions of bandwidth versus fiber length can be obtained for the two scrambler positions and are shown in figure 4, where red and blue continuous lines show the model predictions for the scrambler at the fiber input and output ends, respectively. These predictions were directly calculated and no free parameters were used to fit the model results to the experimental bandwidths.

The plots show an overall agreement between the model and the experimental results, except for some discrepancies for the HFB fiber which can be accounted for by some inherent variability in the measurement conditions such as changes in the scrambler insertion, fiber curvatures or defects, etc. In addition, predictions confirm previous experimental results that show that, when the scrambler is at the input end, the bandwidths are narrower than when the scrambler is near the detector where the scrambler acts as a spatial filter [9, 16, 17, 14]. In summary, we have demonstrated the flexibility of the matricial implementation of the power flow model that can thus accommodate localized disturbances and correctly predict their effects over transmission properties.

4.2. Analysis of scrambler effects for different launching conditions

A similar approach to that described in section 4.1 was followed by changing the source spatial width to calculate the width and frequency bandwidth of the output power distribution for the PGU fiber. In real conditions, the injection width, described as the half-width at half-maximum (HWHM) of the radial profile, can be tailored to be as narrow as 0.5°, reaching up to 60° for a Lambertian source. Commercial sources for POF applications in communications have an HWHM that ranges from 3.5° to 15°, but here we are going to test the whole range from 0.5° to 60° in order to evaluate the asymptotic behavior of the system.

In figure 5, the output HWHM is shown as a function of fiber length for several input HWHMs and three different

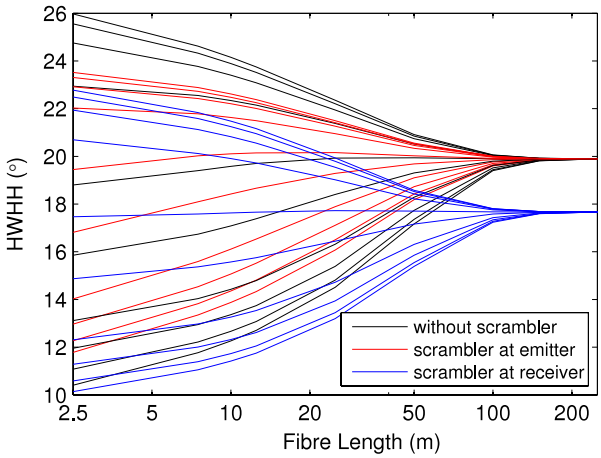

Figure 5. Evolution of the HWHM of the FFP with fiber length. The input source HWHM ranges from 0.5° to 60° from lower to upper lines.

conditions: without a scrambler (black lines), with the scrambler near the transmitter (red lines) and with the scrambler near the detector (blue lines). The curves correspond to increasing injection HWHMs from bottom to top for all three conditions. The condition without a scrambler, with all the curves converging to a value near 20°, shows the effects of propagation over power distribution. For narrow inputs, the input pattern is widened by power diffusion, while wider inputs are narrowed by differential attenuation. The effect of the scrambler near the optical source is to reduce the variation with length, but it is difficult to produce the same output independent on the source and the fiber length. In this case, the distributed effects caused by power propagation dominate over the localized diffusive effects of the scrambler.

On the other hand, when the scrambler is placed at the detector side, it determines the shape of the pattern which reaches a stable level at a narrower width (17°) than in the other two conditions, due to the scrambler spatial filtering that removes the power at high angles.

To analyze the bandwidth enhancement induced by the scrambler spatial filtering, the percentage of bandwidth increment versus input HWHM is shown in figure 6 for four different lengths (12.5, 25, 50 and 100 m). The figure shows

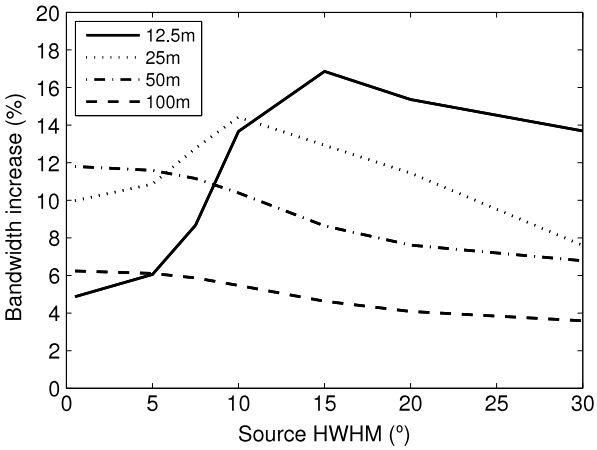

Figure 6. Bandwidth increase versus input HWHM for four fiber lengths.

that the increment is more significant for lengths from 12.5 to 50 m and input HWHMs from 5° to 25°, reaching a maximum of 17% for a 12.5 m fiber with input source HWHM of 15°. Thus, we have shown that this bandwidth increase is always present but it is greater for sources in the range of those used in POF transceivers for communications and fiber lengths suitable for home applications.

5. Conclusions

We have characterized a corrugated scrambler as a matrix, independent of fiber type, that describes power spread over adjacent angles. We predicted bandwidths introducing the scrambler into the matrix propagation model whose agreement with previous experimental data validates the joint scrambler–fiber model. Therefore, we have demonstrated how the matrix power flow equation can be used, not only to model propagation, but can also be extended to introduce localized spatial disturbances in a compact and simple way. Thus, our results reveal the potential of the matrix approach of the power flow equation to study the macroscopic effects of devices, such as scramblers, tappers, etc, and the impact of curvatures and torsion, over light propagation in plastic optical fibers that can be useful when deploying home or car networks.

Acknowledgments

We want to give our special thanks to Demetri Kalymnios, who lent us the scrambler, for his kind comments and useful discussions.

This work was supported by the Spanish Ministry for Science and Technology under grant TEC2009-14718-C03.

References

[1] Gloge D 1972 Optical power flow in multimode fibers *Bell Syst. Tech. J.* **51** 1767–83
[2] Djordjevich A and Savovic S 2000 Investigation of mode coupling in step index plastic optical fibers using the power flow equation *IEEE Photon. Technol. Lett.* **12** 1489–91
[3] Djordjevich A and Savovic S 2004 Numerical solution of the power flow equation in step-index plastic optical fibers *J. Opt. Soc. Am.* B **21** 1437–42
[4] Mateo J, Losada M A and Garcés I 2006 Global characterization of optical power propagation in step-index plastic optical fibers *Opt. Express* **14** 9028–35
[5] Gloge D 1973 Impulse response of clad optical multimode fibers *Bell Syst. Tech. J.* **52** 801–16
[6] Breyer F, Hanik N, Lee S C J and Randel S 2007 *POF Modelling: Theory, Measurement and Application* (Norderstedt: Verlag Books on Demand GmbH) chapter (Getting the Impulse Response of SI-POF by Solving the Time-Dependent Power-Flow Equation using the Crank–Nicholson Scheme)
[7] Mateo J, Losada M A and Zubia J 2009 Frequency response in step index plastic optical fibers obtained from the generalized power flow equation *Opt. Express* **17** 2850–60
[8] Fuster G and Kalymnios D 1998 Passive components in POF data *7th Int. Conf. on Plastic Optical Fibres and Applications* pp 75–80
[9] Mateo J, Losada M A, Martínez-Muro J J, Garcés I and Zubia J 2005 Bandwidth measurement in POF based on general purpose equipment *14th Int. Conf. on Plastic Optical Fibres and Applications* pp 53–6
[10] Koeppen C, Shi R F, Chen W D and Garito A F 1998 Properties of plastic optical fibers *J. Opt. Soc. Am.* B **15** 727–39
[11] Attia R and Marcou J 2000 Mode scrambler for polymer optical fibers *Opt. Eng.* **39** 299–303
[12] Arrue J, Aldabaldetreku G, Durana G, Zubia J, Garcés I and Jiménez F 2005 Design of mode scramblers for step-index and graded-index plastic optical fibers *J. Lightwave Technol.* **23** 1253–60
[13] Mateo J, Losada M A, Garcés I, Arrúe J, Zubia J and Kalymnios D 2003 High NA POF dependence of bandwidth on fibre length *12th Int. Conf. on Plastic Optical Fibres and Applications* pp 123–6
[14] Grivas E, Raptis N and Syvridis D 2010 An optical mode filtering technique for the improvement of the large core SI-POF link performance *J. Lightwave Technol.* **28** 1796–801
[15] Heredia P, Mateo J and Losada M A 2007 Transmission capabilities of large-core gi-pof based on BER measurements *16th Int. Conf. on Plastic Optical Fibres and Applications* pp 307–10
[16] Kalymnios D 1999 Squeezing more bandwidth into high NA POF *8th Int. Conf. on Plastic Optical Fibres and Applications* pp 18–24
[17] Kalymnios D 2003 Increasing the bandwidth of standard high NA SI-POF links *Proc. 2nd Asia Pacific Polymer Fibre* pp 32–6